Eur. Phys. J. A (2018) **54**: 223
DOI 10.1140/epja/i2018-12662-7

THE EUROPEAN PHYSICAL JOURNAL A

Regular Article – Experimental Physics

Phenomenological critical interaction distance from elastic scattering measurements on a ^{208}Pb target

V. Guimarães[1,a], J. Lubian[2], J.J. Kolata[3], E.F. Aguilera[4], M. Assunção[5], and V. Morcelle[6]

[1] Instituto de Física, Universidade de São Paulo, Rua do Matao, 1371, 05508-090 São Paulo, SP, Brazil
[2] Instituto de Física, Universidade Federal Fluminense, Avenida Litoranea s/n, Gragoata, Niteroi, Rio de Janeiro 24210-340, Brazil
[3] Physics Department, University of Notre Dame, Notre Dame, IN, 46556-5670, USA
[4] Departamento de Aceleradores, Instituto Nacional de Investigaciones Nucleares, Apartado Postal 18-1027, Codigo Postal 11801, México, Distrito Federal, Mexico
[5] Departamento de Física, Universidade Federal de São Paulo, Campus Diadema, 09913-030, Diadema, SP, Brazil
[6] Universidade Federal Rural do Rio de Janeiro, 23851-970, Rio de Janeiro, Brazil

Received: 2 October 2018 / Revised: 20 November 2018
Published online: 19 December 2018

Communicated by P. Woods

Abstract. We have surveyed a series of elastic scattering measurements from the literature involving tightly bound (^{9}Li, ^{10}Be, ^{12}C, ^{16}O, ^{19}F), weakly bound (^{6}Li, ^{7}Li, ^{8}Li, ^{8}He, ^{9}Be, ^{17}F), and exotic (^{6}He and ^{11}Li) nuclei on a ^{208}Pb target at energies close to the Coulomb barrier. The corresponding data were then converted and analyzed in terms of the interaction distance, where critical-interaction and strong-absorption distances were extracted. Larger values were obtained for the exotic ^{6}He and ^{11}Li nuclei, as compared with both weakly bound and tightly bound projectiles. The influence of long-range nuclear interactions and Coulomb dipole polarizability are discussed. A correlation between the critical interaction distance and binding energy for a given configuration is observed.

1 Introduction

The investigation of the structure and reactions involving light exotic nuclei has attracted much attention in the last two decades. The interest in such nuclei is due to their quite different properties when compared with those for ordinary nuclei. One of the unusual configurations found in light exotic nuclei occurs when a core nucleus is surrounded by one or more weakly bound valence nucleons. If these are weakly bound to the core the system will have a very diffuse matter distribution at the surface, forming a so-called *halo* configuration in which the loosely bound valence nucleons are found at much greater distances from the core. The nuclear radii of these systems therefore do not follow the conventional $R = r_0 \times A^{1/3}$, with $r_0 \approx 1.25\,\mathrm{fm}$, expression. For a review of the halo structure of exotic nuclei see for instance ref. [1] and references therein.

Nuclei such as ^{11}Li and ^{6}He form *Borromean* systems in which the inert core and two valence neutrons are bound together in such a way that, if any of these objects is removed, the remaining two-body subsystem (core-n or n-n) is unbound. The expression originates from the interlocking Borromean rings [2]. Both halo and Borromean structures differ significantly from that of ordinary nuclei which have a well-defined surface. These geometries (static effects) can strongly influence the several reaction mechanisms induced by such nuclei. The synergy between the structure (static effect) and dynamics (reaction mechanism) is also important. For instance, the weak binding energy of such nuclei makes them easy to break up during the interaction with a target, favoring couplings to the continuum (a dynamic effect) [3,4]. For a review of fusion, breakup and elastic scattering induced by light exotic nuclei see refs. [5–7].

Elastic scattering is the simplest process which can occur in the collision of two nuclei. At low energies, it is a surface process and therefore very useful to investigate the peculiar surface properties of weakly bound exotic nuclei. Analysis of elastic scattering angular distributions measured at energies near the Coulomb barrier can provide valuable information on both the static and dynamics effects of exotic nuclei. Although some progress has been achieved in microscopic reaction theory [8–10], a phenomenological approach, in which the interaction between colliding nuclei is represented by an appropriate

[a] e-mail: valdirg@if.usp.br

optical-model potential, is still a very reliable and practical method to analyze angular distribution data for an elastic-scattering process, and such an analysis can give information about the structure of exotic nuclei.

For ordinary, stable nuclei at energies close to the Coulomb barrier, the elastic scattering is purely Rutherford at forward angles ($\sigma/\sigma_{\rm R} \approx 1$). As the scattering angle increases, a typical Fresnel oscillatory diffraction pattern may appear due to the interference between partial waves refracted by the Coulomb and short-range nuclear potentials. At still larger angles, the absorptive component of the optical-model potential exponentially damps $\sigma/\sigma_{\rm R}$. For lighter projectiles, the Coulomb force is smaller and the diffractive pattern changes from Fresnel to Fraunhofer oscillations, whose period is related to the grazing angular momentum of the collision.

For exotic projectiles, the elastic-scattering angular distribution will show different features. The low binding energy of the valence nucleon(s) may favor breakup during the interaction, due to the Coulomb field of the target and/or possibly a long-range component of the nuclear potential, called the *dynamic polarization potential* (DPP), which reflects the properties of the long tail of the halo-nucleon wave function. The overall effect of this long-range polarization potential is to reduce or eliminate the Fresnel peak and damp the elastic scattering angular distribution at all angles for which the effect of the interaction is felt (see refs. [11–13] for more details). Long-range absorption, responsible for the loss of elastic flux, could be the combination of effects related to both the nuclear and Coulomb interactions, and/or interference between them, depending on the particular structure and/or configuration of the projectile/target. The origin and characteristics of this long-range component is yet to be fully understood.

Distances and radii play important roles in the phenomenological analysis of elastic scattering data. For instance, studies of the threshold anomaly (the relationship of the energy variation of the imaginary and real well depths of the potentials in the vicinity of the barrier [14]) are usually performed at the strong-absorption radius where the elastic scattering is most sensitive to the optical-model potential. For stable and ordinary nuclei, this radius may be defined at to the point where the ratio of elastic scattering to Rutherford drops to 0.25, designated by d_s. The angle at which $\sigma/\sigma_{\rm Ruth} = 0.25$ ($\theta_{1/4}$) is the "grazing angle". For weakly bound and exotic nuclei, with a very diffuse surface, the region of strong sensitivity to the potential is not as easily defined. A previous attempt to map the radial sensitivity was performed by Cramer and deVries [15], by introducing a localized perturbative term in the potential which could be varied as a function of the relative distance of the colliding nuclei. A similar method was applied by MacFarland and Pieper [16]. These two works confirmed that heavy-ion scattering at energies close to the barrier primarily probes the nuclear surface region.

To contribute to this discussion, we have surveyed a series of elastic scattering measurements from the literature involving tightly bound (^{9}Li, ^{10}Be, ^{12}C, ^{16}O, ^{19}F), weakly bound (^{6}Li, ^{7}Li, ^{8}Li, ^{8}He, ^{9}Be, ^{17}F), and exotic (^{6}He and ^{11}Li) nuclei on a ^{208}Pb target at energies close to the Coulomb barrier. The choice of ^{208}Pb as a target is suggested by the fact that it is a spherical, doubly magic nucleus for which very low collectivity is expected. The data were converted and analyzed in terms of the interaction distance, in order to investigate the influence of static and dynamic effects on elastic scattering.

The outline of this paper is as follows. In sect. 2, the procedure to extract the critical interaction distance is described. The values obtained for some nuclei are given in sects. 2.1 and 2.2. In sect. 2.3 we present a discussion about the correlation of critical interaction distance and binding energy of the nuclei. A final discussion and conclusions appear in sect. 3.

2 Critical interaction distance

Static and dynamic effects in the elastic scattering process at low energies can be investigated in a semi-classical approach by plotting the ratio of the elastic cross section to the Rutherford value, $\mathrm{d}\sigma/\mathrm{d}\sigma_{\rm R}$, as a function of the distance of closest approach D on a Rutherford trajectory, which is related to the incident energy and scattering angle in the center of mass (c.m.) frame as

$$D = \frac{1}{2} D_0 \left[1 + \frac{1}{\sin(\theta_{\rm c.m.}/2)} \right], \tag{1}$$

where

$$D_0 = \frac{1}{4\pi\epsilon_0} \frac{Z_P Z_T e^2}{E_{\rm c.m.}} \tag{2}$$

is the distance of closest approach for a head-on collision, with ϵ_0 as the dielectric constant in vacuum.

This classical orbit description can be justified if we consider that the distances D are larger than the De Broglie wavelength for projectiles at energies close to the barrier. In this paper, we consider the $\mathrm{d}\sigma/\mathrm{d}\sigma_{\rm R}$ plot as a function of the "reduced" distance of closest approach given by

$$d = D/\left(A_P^{1/3} + A_T^{1/3} \right). \tag{3}$$

Here and above, $[Z_P, A_P]([Z_T, A_T])$ correspond to the charge and mass numbers of the projectile (target).

One example of such a plot is presented in fig. 1(a) for the $^{16}\mathrm{O} + ^{208}\mathrm{Pb}$ system, where angular distribution data measured at five different incident energies ($E_{\rm Lab}$ = 78, 80, 82, 84 and 86 MeV [17]) have been considered. No deformation-induced effects are expected for this spherical and strongly bound projectile, and $\mathrm{d}\sigma/\mathrm{d}\sigma_{\rm R}$ is close to unity for larger distances but falls off rapidly at short distances due to strong absorption of the elastic flux into non-elastic channels (mostly fusion for this system).

From the $\sigma/\sigma_{\rm R}$ *versus* reduced distance of the closest approach, d, plot we can extract the critical interaction distance, d_I, which is the distance where the nuclear interaction begins to be felt and the cross-section ratio starts deviating from unity. The idea of extracting the interaction distance from elastic scattering measurements dates

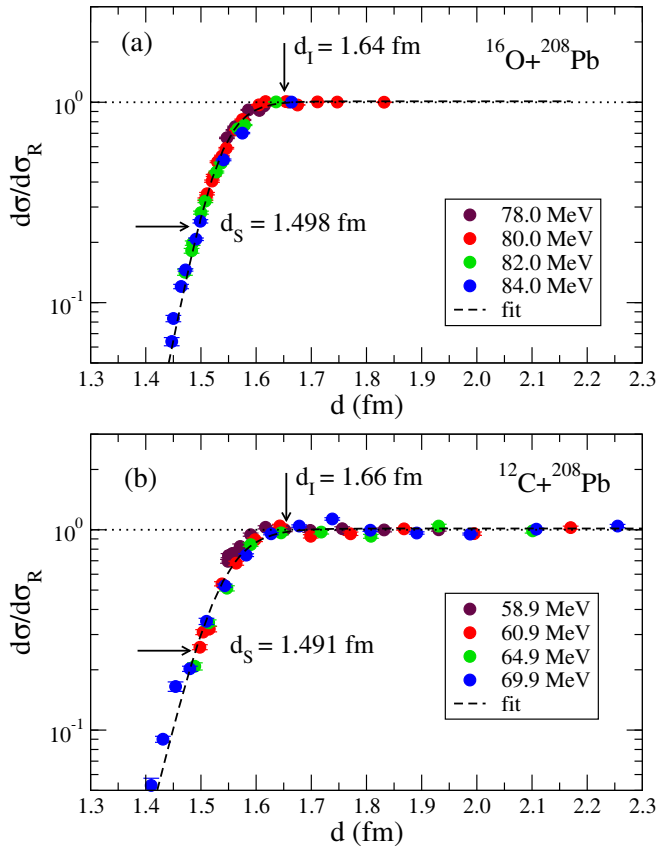

Fig. 1. Ratio of the elastic cross section to the Rutherford value, $d\sigma/d\sigma_R$, as a function of the reduced distance of closest approach d for the (a) $^{16}O+^{208}Pb$ [17] and (b) $^{12}C+^{208}Pb$ [20] systems, at the energies indicated.

to the 70s, when Christensen *et al.* [18] fit straight lines to the two asymptotic regions of $d\sigma/d\sigma_R$ as a function of reduced distance of closest approach. The distance where these lines crossed was defined as the critical interaction distance. Here, we adopt a definition of the critical distance as the point where the ratio of elastic scattering to the Rutherford value is 0.98 or, in other words, when the absolute value of the S-matrix is 0.99. A similar definition was firstly proposed by Pakou and Rusek (ref. [19]), except that they chose a cross-section ratio of 0.97 rather than 0.98.

To more precisely and reliably determine the reduced critical interaction distance, d_I, the procedure of Pakou and Rusek [19] is adopted, where a Boltzmann exponential function is used to fit the cross section data. However, differently from Pakou and Rusek, we consider only three free parameters

$$y = p_1 \times \left[1 + e^{-p_2(d-p_3)}\right]^{-1}, \qquad (4)$$

where $y = d\sigma/d\sigma_R$, d is the reduced distance of the closest approach, and p_1, p_2 and p_3 are adjustable parameters used to fit the data. While this expression has no real physical meaning, it does provide a good fit to the data in the region of interest and therefore enables the extraction of the critical interaction distance, d_I, and reduced strong-absorption distance, d_S, in a consistent and uniform manner.

This fitting procedure was applied to the ^{16}O + ^{208}Pb [17] and $^{12}C+^{208}Pb$ [20] systems with the results illustrated in figs. 1(a) and (b), respectively. The data from the literature were converted from $d\sigma/d\sigma_R$ as a function of angle for a given energy to $d\sigma/d\sigma_R$ as a function of the reduced distance of closest approach, without any additional normalization. It is important to emphasize that we considered only data taken at energies close to the barrier, where a smaller contribution from Fresnel oscillations is expected. The list of the data considered in the present analysis is shown in table 1. The values for the barrier for each system as calculated with the São Paulo Potential [21] are also given. Some data were taken from EXFOR database [22] and some from NRV (Nuclear Reactions Video) database [23] as indicated.

To extract the reduced critical interaction, d_I, and reduced strong-absorption, d_S, distances we applied eq. (4). All three parameters were free to vary during the fitting procedure. The values obtained for the $^{16}O+^{208}Pb$ system were $p_1 = 1.018(2)$, $p_2 = 31.15(8)$ and $p_3 = 1.5333(2)$. The parameter p_1 in eq. (4) is actually the asymptotic value of y for large distance d. This parameter is associated with the asymptotic value of the $d\sigma/d\sigma_R$ data, which should be close to unity for large values of distance d. This parameter is then related to the normalization of the data at forward angles, where the elastic scattering should be purely Rutherford. The values obtained for the parameter p_1 for each of the systems investigated here are also listed in table 1. From the result of the fit we could extract the reduced critical interaction distance, d_I, for which the $d\sigma/d\sigma_R$ ratio is 0.98. This procedure takes into account several cross sections obtained from angular distributions measured at different energies. The quality of the data, related to the uncertainty and in the fluctuation of the cross sections, are also taken into account. Considering this procedure, the reduced critical interaction distance obtained for $^{16}O + ^{208}Pb$ is $d_I = 1.64(1)$ fm, corresponding to a distance $D_I = 13.85(8)$ fm. The uncertainty in d_I was taken to be one-half of the difference from where the ratios are 0.97 and 0.99. For the other strongly bound system, $^{12}C + ^{208}Pb$, shown in fig. 1(b), the reduced critical interaction distance is $d_I = 1.66(1)$ fm, which is the equal within uncertainty as for ^{16}O. We also derive the reduced strong-absorption distance, d_S, for which $d\sigma/d\sigma_R$ ratio is 0.25 and with an uncertainty taken to be one-half the difference from where the ratios are 0.24 and 0.26. The reduced strong-absorption distance is found to be $d_S = 1.498(2)$ fm for $^{16}O + ^{208}Pb$, corresponding to $D_S = 12.70(2)$ fm, and $d_S = 1.491(2)$ fm for $^{12}C + ^{208}Pb$, corresponding to $D_S = 12.24(2)$ fm. Again the reduced strong-absorption distances are about the same for both ^{12}C and $^{16}O + ^{208}Pb$ systems. For these tightly bound projectiles, both reduced strong-absorption and critical interaction distances are small, being in the range of 1.45–1.55 fm and 1.60–1.70 fm, respectively. The difference between these two distances is $\Delta d = d_I - d_S = 0.14$ for ^{16}O and 0.17 for ^{12}C. Direct processes (inelastic excitation,

Table 1. The reduced critical interaction distance, d_I, and the reduced strong-absorption distance, d_S (at which $\mathrm{d}\sigma/\mathrm{d}\sigma_{Ruth}$ are 0.98 and 0.25, respectively) for the projectiles indicated. The cluster configuration of the projectile and the corresponding binding energy are also listed. Δd is the difference between the distances d_I and d_S.

	Reference	B.E. (MeV)	V_B (MeV)	d_I (fm)	p_1	d_S (fm)	Δd
^{6}He	S.-Benitez-05 [33][(a)]	0.973 (^{4}He + 2n)	19.1	2.20(5)	0.999(1)	1.589(7)	0.61
	Kakuee-06 [34][(a)]						
^{8}He	M.-Duran-16 [35][(a)]	2.140 (^{6}He + 2n)	18.6	2.24(7)	1.000(3)	1.718(6)	0.52
^{6}Li	Keeley-94 [32][(a)]	1.474 (^{4}He + d)	29.4	1.95(4)	1.007(1)	1.521(5)	0.43
^{7}Li	Keeley-94 [32][(a)]	2.467 (^{4}He + t)	29.0	1.74(2)	1.019(1)	1.491(3)	0.25
^{8}Li	Kolata-02 [25][(a)]	2.032 (^{7}Li + n)	28.7	2.30(7)	0.993(6)	1.651(7)	0.55
^{9}Li	Cubero-12 [13][(c)]	4.064 (^{8}Li + n)	28.3	1.84(3)	1.003(1)	1.522(3)	0.32
^{11}Li	Cubero-12 [13][(a)]	0.369 (^{9}Li + 2n)	27.8	5.16(44)	0.999(2)	1.59(4)	3.57
^{7}Be	Mazzocco-17 [26][(c)]	1.587 (^{4}He + ^{3}He)	39.4	1.86(5)	0.996(3)	1.509(4)	0.35
^{9}Be	Yu-10 [29][(a)]	1.655 (^{8}Be + n)	38.9	1.86(2)	1.005(2)	1.540(4)	0.31
^{10}Be	Kolata-04 [27][(a)]	6.812 (^{9}Be + n)	38.1	1.73(2)	1.012(3)	1.521(2)	0.21
^{12}C	Santra-01 [20][(a)]	7.367 (^{8}Be + α)	57.6	1.66(1)	1.014(3)	1.491(2)	0.17
^{16}O	Vulgaris-86 [17][(c)]	7.162 (^{12}C + α)	76.0	1.64(1)	1.012(4)	1.498(2)	0.14
^{17}F	Liang-03 [28][(a)]	0.601 (^{16}O + p)	85.5	1.69(1)	1.031(2)	1.491(3)	0.20
^{19}F	Lin-01 [36][(b)]	4.014 (^{15}N + α)	84.5	1.63(2)	1.008(5)	1.489(2)	0.14

[(a)] Data sets obtained from EXFOR database [22].
[(b)] Data sets obtained from the *NRV* database [23].
[(c)] Data sets obtained from the figures of the original papers by the authors of the present paper.

breakup, transfer etc.) are the main cause of flux absorption from elastic scattering in the region between these two distances for the ^{16}O projectile, as discussed by Kim *et al.* [24].

The idea of the present work is to compare the reduced critical interaction and strong-absorption distances for different projectile types (exotic, weakly and strongly bound, stable and radioactive light nuclei) on the same target. To do that, we follow and extend the work of Pakou and Rusek in ref. [19] by analyzing data from several other projectiles, including tightly bound (^{9}Li, ^{10}Be, ^{12}C, ^{16}O, ^{19}F), weakly bound (^{6}Li, ^{7}Li, ^{8}Li, ^{8}He, ^{9}Be, ^{17}F) and exotic (^{6}He and ^{11}Li) nuclei on a ^{208}Pb target. It is important to mention that the data from the literature were directly converted from $\mathrm{d}\sigma/\mathrm{d}\sigma_{\mathrm{R}}$ as a function of angle for a given energy to $\mathrm{d}\sigma/\mathrm{d}\sigma_{\mathrm{R}}$ as a function of distance. Also, all the data were obtained at energies close to the Coulomb barrier where the Fresnel peak is not pronounced, allowing a fit using eq. (4). Such a procedure allows the combination of several data set, distributed in terms of angular distribution ($\mathrm{d}\sigma/\mathrm{d}\sigma_{\mathrm{R}}$ *versus* $\Theta_{\mathrm{c.m.}}$), into one data set ($\mathrm{d}\sigma/\mathrm{d}\sigma_{\mathrm{R}}$ *versus* d). For radioactive projectile data, where cross sections were obtained at fewer angles for each energy but at several different energies, this procedure has been shown to be of particular utility, for instance for ^{8}Li [25], ^{7}Be [26], ^{10}Be [27] and ^{17}F [28].

To check for any possible energy dependence in the extraction of the reduced critical distance, we considered the data for the ^{9}Be + ^{208}Pb system from Yu *et al.* [29]. This data set has very good quality and the angular distributions were measured at several energies ranging from 38.0 to 50 MeV. Using the procedure described above, we obtained the critical interaction distance d_I considering data for each angular distribution. The results for the parameter p_1 and for the critical distance of interaction are listed in table 2. As one can see, the obtained values for the parameter p_1 are close to unity, indicating a good normalization of the data. Also the values for the d_I are consistent with each other within error, yielding an average value of $\langle d_I \rangle = 1.85(2)$ fm. The energy dependence can be considered to be negligible for this particular range. The good quality of the cross-section data obtained at several angles and for several energies are reflected in the plot of fig. 2, with small fluctuations in the cross section as

Table 2. The parameter p_1 and the reduced critical interaction distance d_I for the ^{9}Be + ^{208}Pb system at the different energies indicated.

Energy (MeV)	p_1	d_I (fm)
38.0	1.001(3)	1.87(2)
39.0	1.009(3)	1.83(2)
40.0	1.000(3)	1.86(2)
41.0	1.004(3)	1.85(2)
42.0	1.004(3)	1.85(2)
44.0	1.014(3)	1.83(2)
50.0	1.001(3)	1.86(2)

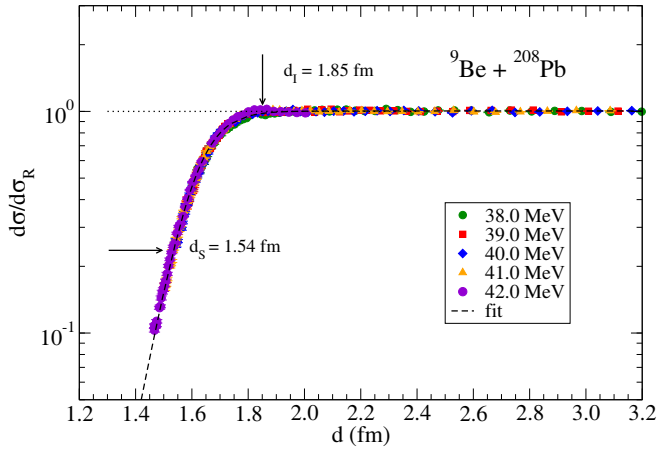

Fig. 2. Ratio of the elastic cross section to the Rutherford value, $d\sigma/d\sigma_R$, as a function of the reduced distance of closest approach d for the ^{9}Be + ^{208}Pb system, at the energies indicated. The data are taken from ref. [29].

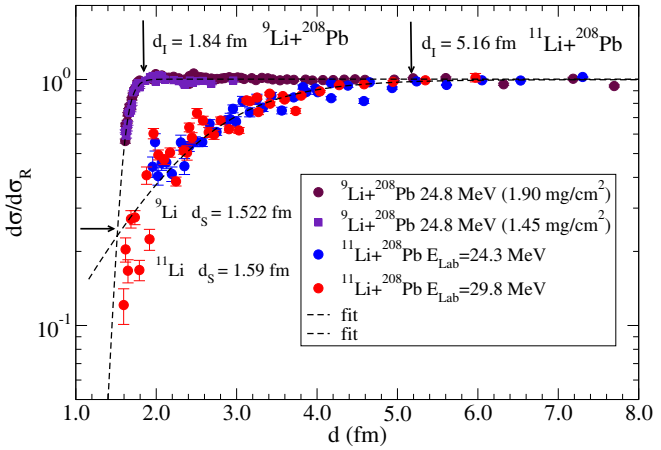

Fig. 3. Ratio of elastic cross section to the Rutherford value, $d\sigma/d\sigma_R$, as a function of the reduced distance of closest approach d for the ^{9}Li and ^{11}Li + ^{208}Pb systems, at the energies indicated. The data are taken from ref. [13].

a function of the distance of closest approach. The critical distance of interaction obtained for the combination of the data from 38.0 to 42.0 MeV is $d_I = 1.86(2)$ fm for this system, which is about the same as the average obtained by considering angular distributions from 38.0 to 50 MeV. This value is somewhat larger than that for the tightly bound nuclei ^{12}C and ^{16}O. On the other hand, the reduced strong-absorption distance for this system is found to be $d_S = 1.540(4)$ fm, which is in the same range of 1.45–1.55 fm obtained for ^{12}C and ^{16}O. Considering the lower binding energy for ^{9}Be, this may be an indication that direct reactions, such as breakup and transfer, start playing a role for this system at distances larger than that for tightly bound nuclei.

2.1 Distances for ^{6,7,8,9,11}Li projectiles

Following the prescription described in the previous section, we analyzed elastic scattering data for ^{9}Li and ^{11}Li [13] on a ^{208}Pb target. The cross-section ratios *vs.* the reduced distance of closest approach for these systems are shown in fig. 3. The dashed curves correspond to the fits using eq. (4), and the reduced critical interaction distances obtained for each isotope are indicated. For the exotic borromean nucleus ^{11}Li the reduced critical distance is quite large, $d_I = 5.16(44)$ fm, when compared to that for ^{9}Li, $d_I = 1.84(3)$ fm. The reduced strong-absorption distances for both ^{9}Li and ^{11}Li are about the same, $d_S = 1.522(3)$ and $1.59(4)$ fm, and are quite similar to those for ^{6}He, ^{6}Li, ^{7}Be, ^{9}Be. The difference between the reduced critical interaction and strong-absorption distances, Δd, is 3.57 and 0.32 fm, for ^{11}Li and ^{9}Li, respectively. The larger value of the difference between the distances can be interpreted as due to the combination of a static effect, the extended matter distribution and borromean cluster configuration of ^{11}Li, as well as dynamic effects such as a lower breakup threshold inducing couplings to direct channels. The extended direct-interaction region for the ^{11}Li projectile corroborates the importance of the long-range Coulomb and/or nuclear interaction for this exotic projectile, as also observed in the reduction of the Fresnel diffraction peak in the corresponding angular distributions [13]. In the case of ^{11}Li, the much larger difference as compared to any other projectile analyzed here can be attributed to the much stronger dynamic polarizability of this nucleus which can give rise to a long-range Coulomb interaction. The effect of this strong polarizability, which is almost certain to be due to the presence of the strong soft electric dipole at low excitation energy [30] in ^{11}Li, would be to reduce the elastic-scattering cross sections even at energies well below the barrier [13,31].

For the weakly bound lithium isotopes ^{6,7,8}Li + ^{208}Pb we used the data for ^{6}Li and ^{7}Li from ref. [32] and for ^{8}Li from ref. [25]. In fig. 4 the plots for the $d\sigma/d\sigma_R$ *versus* d for ^{6}Li and ^{8}Li are shown. The obtained critical interaction and strong interaction distances for these isotopes are listed in table 1. The reduced critical interaction distances are larger for these weakly bound nuclei in comparison with those obtained for the tightly bound nuclei ^{12}C and ^{16}O, while the reduced strong interaction distances are about the same. The large value of the reduced critical interaction distance, $d_I = 2.30(7)$ fm, and reduced strong-absorption distance, $d_S = 1.651(7)$ fm, for the ^{8}Li projectile is somewhat surprising. However, it has to be pointed out that the angular distributions for ^{8}Li have fewer data points and bigger error bars in the region of the critical interaction distance. It is a radioactive projectile and the statistics of the experiment is much lower than that for stable weakly bound projectiles like ^{6,7}Li. The difference between the reduced critical interaction and strong absorption distances, also shown in table 1, are still in the range of those for other weakly bound nuclei. The larger values for the weakly bound nuclei, compared to those $\Delta d \approx 0.15$ for tightly bound nuclei, are mostly due to the influence of direct reactions, such as breakup and transfer, which are important processes that start playing a role at larger distances.

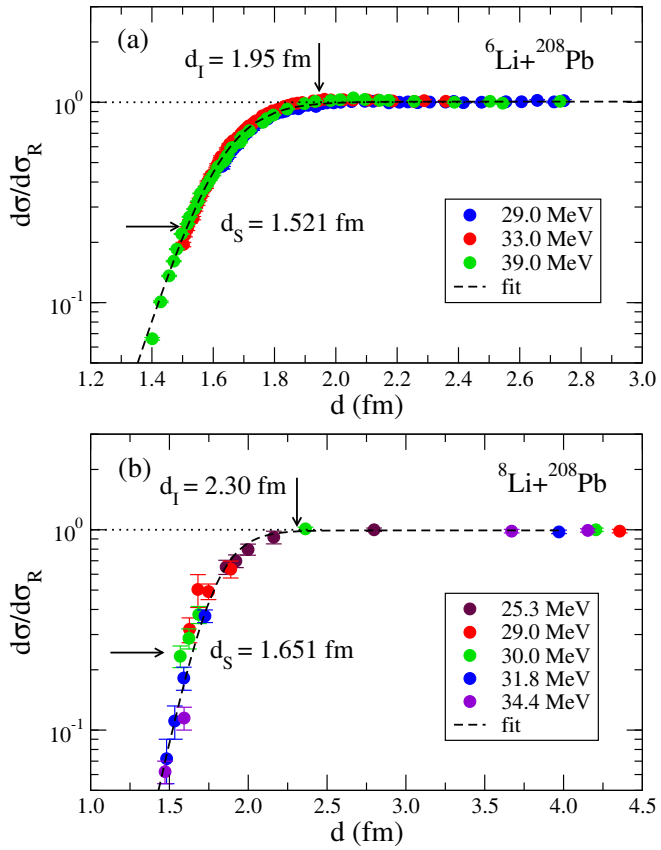

Fig. 4. Ratio of elastic cross section to the Rutherford value, $d\sigma/d\sigma_R$, as a function of the reduced distance of closest approach d for the (a) ^{6}Li + ^{208}Pb [32] and (b) ^{8}Li + ^{208}Pb [25] systems, at the energies indicated.

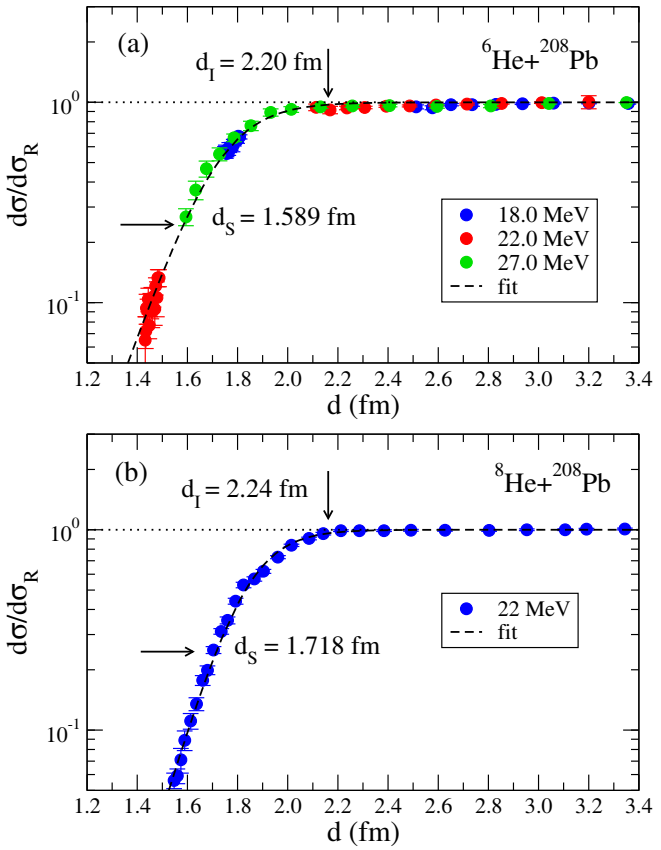

Fig. 5. Ratio of elastic cross section to the Rutherford value, $d\sigma/d\sigma_R$, as a function of the reduced distance of closest approach d for the (a) ^{6}He+^{208}Pb [33,34] and (b) ^{8}He+^{208}Pb [35] systems, at the energies indicated.

2.2 Distances for ^{6,8}He, ^{7,9,10}Be and ^{17,19}F projectiles

Table 1 is completed with results from analyses of data for several other projectiles such as ^{6}He [33,34], ^{8}He [35], ^{7}Be [26], ^{10}Be [27], ^{17}F [28] and ^{19}F [36].

For the exotic borromean nucleus ^{6}He and the weakly bound nucleus ^{8}He, the reduced critical distances are large, $d_I = 2.20(5)$ fm and $d_I = 2.24(5)$ fm, respectively, as shown in fig. 5. Considering the difference with respect to the reduced strong-absorption distance we have $\Delta d = 0.61$ and 0.52 fm for these nuclei, respectively. The large difference for ^{6}He can be attributed to the static and dynamic effects including the extended-matter distribution and lower breakup threshold inducing couplings to direct channels. Although the binding energy for ^{8}He is not as low as for ^{6}He, it seems that similar effects are playing a role for this nucleus as well.

Although ^{8}Li and ^{8}He have different cluster configurations, they have very similar reduced critical distances of interaction, $d_I = 2.23(6)$ and 2.25(7) fm, respectively. The larger value of the reduced critical interaction distance obtained for ^{8}Li among the lithium isotopes ^{6,8,9}Li could be explained as the combination of effects due to cluster configuration and breakup threshold energy. The valence particle of the ^{8}Li isotope is a neutron, while ^{6}Li and ^{7}Li have charged valence particles (deuteron and triton, respectively). Both ^{8}Li and ^{9}Li have a neutron valence particle and the larger value of the reduced critical interaction distance observed for ^{8}Li could be understood as the effect of the lower binding energy for $^8\text{Li} = {}^7\text{Li} + \text{n}$ (2.032 MeV) as compared to $^9\text{Li} = {}^8\text{Li} + \text{n}$ (4.064 MeV). It should be mentioned that the quadrupole moment for the ^{8,9,11}Li isotopes are about the same [37].

The comparison of the $d\sigma/d\sigma_R$ *versus* d plots for ^{7}Be and ^{10}Be is shown in fig. 6. Although these nuclei have approximately the same reduced critical interaction distance, they have completely different cluster configurations and binding energies. The reduced critical interaction distance for ^{7}Be is in the same range 1.80–1.90 as the other weakly bound nuclei, ^{6}Li and ^{9}Be. The data for ^{10}Be constitute a typical example of the advantage of this procedure, where we are able to combine several cross sections measured at relatively few angles but at different energies.

The $d\sigma/d\sigma_R$ *versus* d plots for ^{17}F and ^{19}F nuclei are shown in fig. 7. For the ^{17}F projectile we considered the data taken at 120 MeV. Although ^{17}F has a small binding energy (0.601 MeV), its valence proton particle suffers the influence of a Coulomb barrier plus a higher centrifugal barrier ($l = 2$) since it is located in the $1d_{5/2}$ orbit. The data for ^{19}F also suffers from large fluctuations, but the

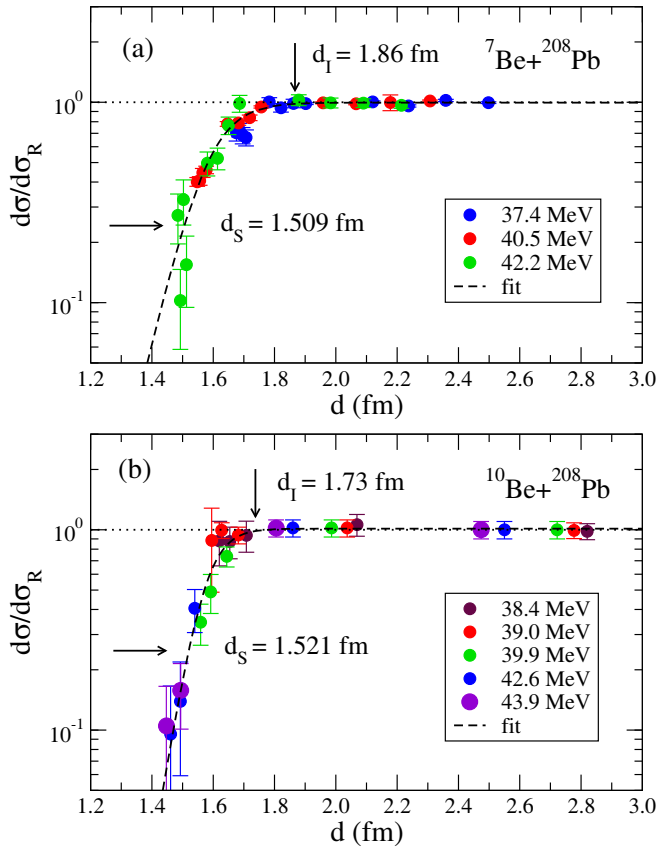

Fig. 6. Ratio of elastic cross section to the Rutherford value, $d\sigma/d\sigma_R$, as a function of the reduced distance of closest approach d for the (a) ^{7}Be + ^{208}Pb [26] and (b) ^{10}Be + ^{208}Pb [27] systems, at the energies indicated.

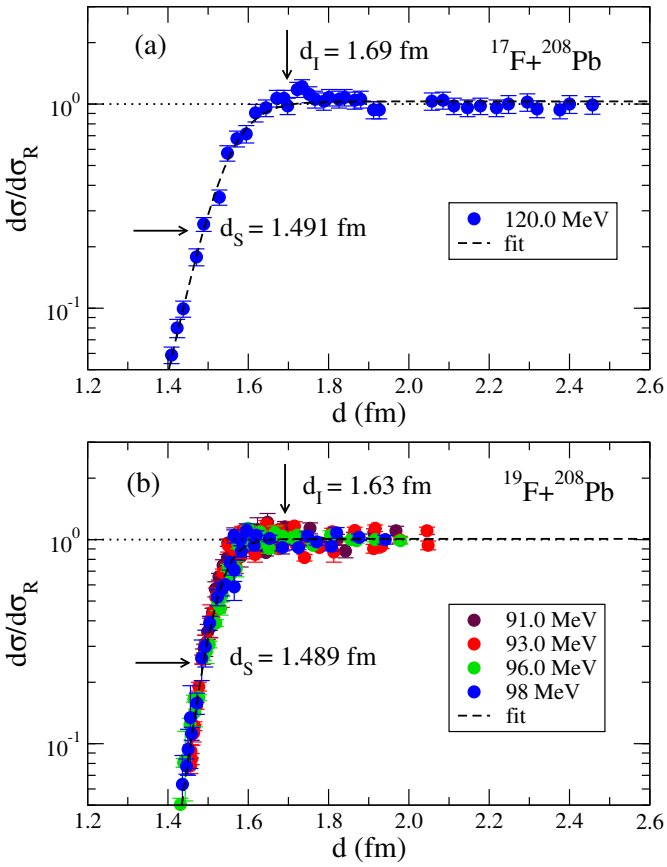

Fig. 7. Ratio of elastic cross section to the Rutherford value, $d\sigma/d\sigma_R$, as a function of the reduced distance of closest approach d for the (a) ^{17}F + ^{208}Pb [28] and (b) ^{19}F + ^{208}Pb [36] systems, at the energies indicated.

combination of all data sets from the angular distributions taken at different energies still allows for the analysis to be made.

2.3 Critical interaction distance and binding energy

Considering the data analyzed here, there is an indication of a possible correlation between the reduced critical interaction distances, given in table 1, and the breakup threshold energy (binding energy of the given cluster configuration) of the projectiles. The plot of the critical interaction distances obtained in this work, as a function of the binding energy for the configuration indicated in table 1, is shown in fig. 8. First we performed a fit (dashed curve in fig. 8) considering only the weakly and tightly bound nuclei, ^{6}Li, ^{7}Li, ^{9}Li, ^{7}Be, ^{9}Be, ^{10}Be, ^{12}C, ^{16}O and ^{19}F. As can be observed in this figure, the more weakly bound the projectile the larger the critical interaction distance.

The other nuclei analyzed in this work, ^{6}He, ^{8}He, ^{8}Li, ^{11}Li and ^{17}F, deviate from the phenomenological dashed curve in fig. 8. First and most obvious is the case of ^{11}Li, which illustrates how strongly the unique structure of this nucleus influences its reaction mechanisms. Unfortunately, there are very few nuclei having a similar structure to compare with, the obvious choice being ^{11}Be (B.E. = 0.501 MeV). It would also be interesting to have elastic scattering measurements at energies close to the barrier for projectiles with binding energies smaller than 1.0 MeV, such as ^{15}C (0.740 MeV), and for proton-rich nuclei such as ^{8}B (0.138 MeV) and ^{12}N (0.601 MeV). Measurements for the last two have been proposed.

Next is the case of ^{17}F, which is a proton-rich nucleus. Despite its low binding energy, the reactions of this nucleus are likely being inhibited by the proton Coulomb barrier and the high angular momentum in its ground state. Its first excited state, which has low spin and a much lower binding energy, has been suggested to be a proton halo system. However, the short mean-life of less than 0.5 ns would make a study of its reactions very difficult to carry out. The elastic data for the ^{17}F ground state were obtained from the work of Liang *et al.* [28]. In the same work, they also report a breakup measurement at the same energy, 120 MeV. The authors concluded that, at this energy, the integrated breakup (BU) cross section was small (one third of the fusion cross section at the same energy) and they concluded from calculations that transfer was negligible at this energy. This conclusion is corroborated by the small interaction distance obtained in this work. Similar conclusions about the small effect of BU and transfer channel on fusion and elastic scattering have

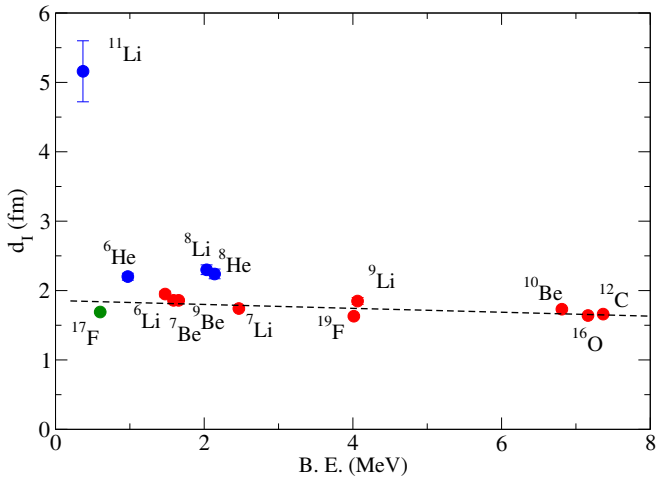

Fig. 8. Reduced critical distance of interaction as a function of the binding energy for the nuclei indicated. The dashed curve indicates the trend of the data for the weakly and tighly bound nuclei in red.

recently been given for the ^{17}F + ^{89}Y system in ref. [38] supporting the results derived here.

Further there are ^{6,8}He, both of which have been shown to have a neutron halo structure [1] so their larger interaction radii are not unexpected. Finally, there is the case of ^{8}Li, which shows an unexplained deviation from the curve. This is quite surprising since its fusion cross section appears to be normal [39] so the increased interaction radius, if real, must be due to peripheral reactions. On the other hand, the total reaction cross section for ^{8}Li on the medium mass nucleus, ^{90}Zr, was found to be anomalously high [40]. Forthcoming study of the ^{8}Li + ^{208}Pb system would therefore be quite interesting.

Although the critical interaction distances obtained here have some relationship to the size of the nuclei, they are also influenced by the reaction mechanisms. This is especially the case for the halo nuclei, where there is a clear departure from an $A^{1/3}$ proportionality of the radii. At distances between critical interaction and strong absorption the mechanisms are predominantly inelastic and other direct channels, while distances smaller than strong-absorption are dominated by fusion. The critical interaction distances can also depend on the nuclear properties, such as the nuclear radius itself, isospin symmetry, binding energy per nucleon, and binding energy of valence particles in a particular cluster configuration, all of which may affect the strength of the couplings for different incident energies.

3 Summary

Static and dynamic effects in the elastic scattering process at low energies were investigated in a semi-classical approach by plotting the ratio of elastic cross section to the Rutherford value as a function of the distance of the closest approach on a Rutherford trajectory. Critical-interaction and strong-absorption distances were extracted from elastic data for several systems from the literature involving tightly bound (^{10}Be, ^{12}C, ^{16}O, ^{19}F), weakly bound (^{6}Li, ^{7}Li, ^{7}Be, ^{8}Li, ^{8}He, ^{9}Be, ^{17}F) and exotic (^{6}He and ^{11}Li) nuclei on a ^{208}Pb target, at energies close to the Coulomb barrier. Larger values of the critical interaction distance were observed for the exotic ^{6}He and ^{11}Li nuclei as compared with the weakly bound ^{6}Li, ^{7}Li, ^{7}Be, ^{8}Li, ^{9}Be nuclei, and even more so when compared with tightly bound projectiles such as ^{10}Be, ^{12}C and ^{16}O. The significantly larger value obtained for ^{11}Li can be understood as due to the influence of the large Coulomb dipole polarizability of this nucleus. The combination of the effect of the large value of the Coulomb dipole polarizability, as well as the large transfer/breakup probabilities observed experimentally, can also be the reason for the large value of the interaction distance for ^{6}He as compared to ^{6}Li. In the present analysis, a correlation between the critical interaction distance and the breakup threshold energy for a given cluster configuration was also observed.

VG would like to thank the São Paulo Research Foundation (FAPESP) (Grants 2016/02863-4 and 2016/17612-7) and the Conselho Nacional de Desenvolvimento Científico (CNPq) (Grant 304961/2017-5) for the financial support. VM thanks FAPERJ and JL thanks CNPq and FAPERJ. VG and JL thank INCT-FNA. This work was partially supported by the U.S. National Science Foundation under Grants No. PHY14-01343 and PHY14-01242 and by CONACYT (México) under grant No. CB-01-254619.

References

1. I. Tanihata, H. Savajols, R. Kanungo, Prog. Part. Nucl. Phys. **68**, 215 (2013).
2. `wikipedia.org/wiki/Borromean_rings`
3. O.A. Rubtsova, V.I. Kukulin, A.M. Moro, Phys. Rev. C **78**, 034603 (2008).
4. P. Capel, F.M. Nunes, J. Phys.: Conf. Ser. **312**, 082015 (2011).
5. J.J. Kolata, V. Guimarães, E.F. Aguilera, Eur. Phys. J. A **53**, 123 (2016).
6. N. Keeley, N. Alamanos, K.W. Kemper, K. Rusek, Prog. Part. Nucl. Phys. **63**, 396 (2009).
7. L.F. Canto, P.R.S. Gomes, R. Donangelo, J. Lubian, M.S. Hussein, Phys. Rep. **596**, 1 (2015).
8. P. Descouvemont, Phys. Rev. C **93**, 034616 (2016).
9. P. Descouvemont, D. Baye, Rep. Prog. Phys. **73**, 036301 (2010).
10. Bao-An Li, Lie-Wen Chen, Che Ming Ko, Phys. Rep. **464**, 113 (2008).
11. V. Morcelle *et al.*, Phys. Lett. B **732**, 228 (2014).
12. A. Di Pietro *et al.*, Phys. Rev. C **85**, 054607 (2012).
13. M. Cubero *et al.*, Phys. Rev. Lett. **109**, 262701 (2012).

14. C. Mahaux, H. Ngo, G.R. Satchler, Nucl. Phys. A **449**, 354 (1986).
15. J.G. Cramer, R.M. DeVries, Phys. Rev. C **22**, 91 (1980).
16. M.H. MacFarlane, S.C. Pieper, Phys. Lett. B **103**, 169 (1981).
17. E. Vulgaris, L. Grodzins, S.G. Steadman, R. Ledoux, Phys. Rev. C **33**, 2017 (1986).
18. P.R. Christensen, V.I. Manko, F.D. Becchetti, R.J. Nickles, Nucl. Phys. A **207**, 33 (1973).
19. A. Pakou, K. Rusek, Phys. Rev. C **69**, 057602 (2004).
20. S. Santra, P. Singh, S. Kailas, A. Chatterjee, A. Shrivastava, K. Mahata, Phys. Rev. C **64**, 024602 (2001).
21. L.C. Chamon, B.V. Carlson, L.R. Gasques, D. Pereira, C. De Conti, M.A.G. Alvarez, M.S. Hussein, M.A. Candido Ribeiro, E.S. Rossi Jr., C.P. Silva, Phys. Rev. C **66**, 014610 (2002).
22. V.V. Zerkin, B. Pritychenko, Nucl. Instrum. Methods Phys. Res. A **888**, 31 (2018).
23. `nrv.jinr.ru/nrv/`.
24. B.T. Kim, W.Y. So, S.W. Hong, T. Udagawa, Phys. Rev. C **65**, 044607 (2002).
25. J.J. Kolata *et al.*, Phys. Rev. C **65**, 054616 (2002).
26. Mazzocco, EPJ Web of Conferences **163**, 00035 (2017).
27. J.J. Kolata E.F. Aguilera, F.D. Becchetti, Yu Chen, P.A. DeYoung, H. Garcia-Martinez, J.D. Hinnefeld, J.H. Lupton, E. Martinez-Quiroz, G. Peaslee, Phys. Rev. C **69**, 047601 (2004).
28. J.F. Liang *et al.*, Phys. Rev. C **67**, 044603 (2003).
29. N. Yu *et al.*, J. Phys. G **37**, 075108 (2010).
30. E.C. Pinilla, P. Descouvemont, D. Baye, Phys. Rev. C **85**, 054610 (2012).
31. J.P. Fernández-García, M.A.G. Alvarez, L.C. Chamon, Phys. Rev. C **92**, 014604 (2015).
32. N. Keekey *et al.*, Nucl. Phys. A **571**, 326 (1994).
33. A.M. Sanchez-Benítez *et al.*, J. Phys. G: Nucl. Part. Phys. **31**, S1953 (2005).
34. O.R. Kakuee *et al.*, Nucl. Phys. A **765**, 294 (2006).
35. G. Marquínez-Durán *et al.*, Phys. Rev. C **94**, 064618 (2016).
36. C.J. Lin, J.C. Xu, H.Q. Zhang, Z.H. Liu, F. Yang, L.X. Lu, Phys. Rev. C **63**, 064606 (2001).
37. D. Borremans *et al.*, Phys. Rev. C **72**, 044309 (2005).
38. G.L. Zhang *et al.*, Phys. Rev. C **87**, 044618 (2018).
39. E.F. Aguilera *et al.*, Phys. Rev. C **80**, 044605 (2009).
40. A. Pakou, Eur. Phys. J. A **55**, 51 (2015).